

Phosphorane–Iminato Complexes of Transition Metals with Heterocubane Structure: A Computational Study

Andreas Sundermann and Wolfgang W. Schoeller*

Contribution from the Fakultät für Chemie, Universität Bielefeld, Postfach 100131, 33501 Bielefeld, Germany

Received August 9, 1999. Revised Manuscript Received March 6, 2000

Abstract: The electronic structure of phosphorane–iminato complexes of transition metals is studied by means of ab initio/DFT methods. Accordingly, the transition metal nitrogen bond is best described as an ionic interaction between a transition metal complex fragment and the strongly polarized NPH_3^- ligand. By elaborate MCSCF calculations a weak antiferromagnetic coupling of the four transition metal centers in the cubane core is predicted. This coupling can be represented by a simple Heisenberg Hamiltonian.

1. Introduction

Since the first synthesis of iminophosphoranes by Staudinger and Meyer¹ at the beginning of this century and the early work of Schmidbaur et al. on compounds of the phosphorane–iminato ion,^{2,3} a large number of main group⁴ and transition metal compounds^{5,6} could be characterized. By reaction of *N*-silylphosphane–imines with halides of transition metals of the 3d series in their formal oxidation state +2, heterocubane structures are formed. Complexes of manganese,^{7–9} iron,⁹ cobalt,^{7,10,11} nickel,^{8,12} zinc,^{11,13,14} and the 4d element cadmium¹⁵ have been characterized by crystal structure determination. Recently, a review has been published on this subject.⁶ All these heterocubane structures are reported to have a nearly ideal cubic $[\text{M}_4\text{N}_4]$ core. As depicted in Figure 1, such molecules can be described as a tetrahedron formed by four transition metal ions. Each face of this tetrahedron is capped by a μ_3 -bridging NPR_3^- ligand. The coordination sphere of the metal ions is saturated by a coordinated halide ion (we have chosen $\text{Hal} = \text{Br}$ for our study). In the case of $\text{R} = \text{H}$, and the quantum chemical considerations given here are restricted to this simplification, the molecular symmetry is D_{2d} .

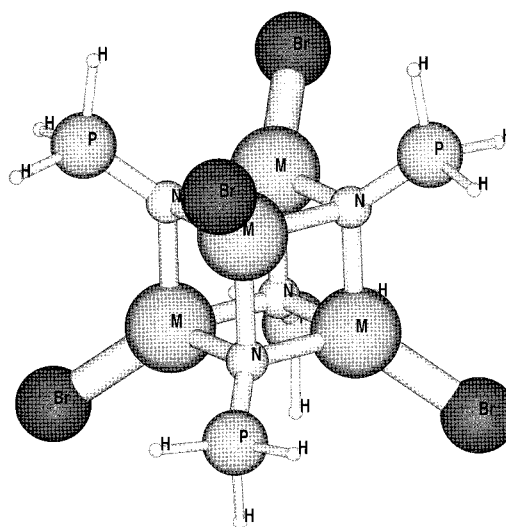


Figure 1. Molecular structure (visualized using the program *MOLDEN*³⁴) of a heterocubane cluster $[\text{MBr}(\text{NPH}_3)]_4$.

Some interesting bonding features of these heterocubane complexes are worthwhile to be considered from a quantum chemical point of view.

1. The N–P bonds are surprisingly short. Are they single or double bonds?

2. All heterocubanes of open shell transition metal ions (i.e. Mn(II), Fe(II), Co(II), and Ni(II)) show reduced magnetic moments at room temperature in comparison with the corresponding spin-only values. Is there some amount of M–M bonding in the cubane core?

3. Is it possible to account for these findings by a computational study on a molecule the size of a heterocubane cluster?

All these questions will be studied in the following quantum chemical investigation. The details of the quantum chemical methodology are given in section 3.

2. Qualitative Considerations

2.1. The Electronic Structure of the NPH_3^- Ligand. The free phosphorane–iminato ion has C_{3v} symmetry. A qualitative description of its electronic structure (Figure 2) can be obtained

* Address correspondence to this author.

- (1) Staudinger, H.; Meyer, J. *Helv. Chim. Acta* **1919**, 2, 635–646.
- (2) Schmidbaur, H.; Wolfsberger, W. *Chem. Ber.* **1967**, 100, 1000–1015.
- (3) Schmidbaur, H.; Jonas, G. *Chem. Ber.* **1968**, 101, 1271–1285.
- (4) Dehnicke, K.; Weller, F. *Coord. Chem. Rev.* **1997**, 158, 103–169.
- (5) Dehnicke, K.; Strähle, J. *Polyhedron* **1989**, 8, 707–726.
- (6) Dehnicke, K.; Krieger, M.; Massa, W. *Coord. Chem. Rev.* **1999**, 182, 19–65.
- (7) Mai, H.-J.; zu Köcker, R. M.; Wocadlo, S.; Dehnicke, K. *Angew. Chem.* **1995**, 107, 1349–1350.
- (8) Mai, H.-J.; Kang, H.-C.; Wocadlo, S.; Massa, W.; Dehnicke, K. *Z. Anorg. Allg. Chem.* **1995**, 621, 1963–1968.
- (9) Riese, U.; Faza, N.; Harms, K.; Massa, W.; Neumüller, B.; Dehnicke, K. *Phosphorus, Sulfur and Silicon* **1997**, 124, 315–321.
- (10) Riese, U.; Harms, K.; Neumüller, B.; Dehnicke, K. *Z. Anorg. Allg. Chem.* **1998**, 624, 1279–1284.
- (11) Abram, S.; Abram, U.; zu Köcker, R. M.; Dehnicke, K. *Z. Anorg. Allg. Chem.* **1996**, 622, 866–872.
- (12) Krieger, M.; Gould, R. O.; Pebler, J.; Dehnicke, K. *Z. Anorg. Allg. Chem.* **1998**, 624, 781–786.
- (13) Krieger, M.; Harms, K.; Magull, J.; Dehnicke, K. *Z. Naturforsch.* **1997**, 52b, 243–250.
- (14) Krieger, M.; Gould, R. O.; Neumüller, B.; Harms, K.; Dehnicke, K. *Z. Anorg. Allg. Chem.* **1998**, 624, 1434–1442.
- (15) Harms, K.; Merle, J.; Maichle-Mössner, C.; Massa, W.; Krieger, M. *Inorg. Chem.* **1998**, 37, 1099–1104.

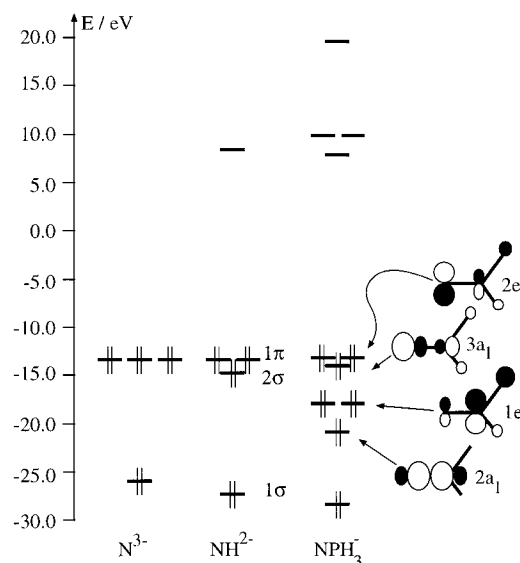
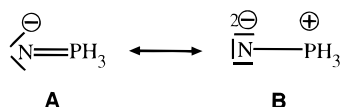


Figure 2. Schematic representation of the frontier orbitals of the phosphorane-iminato ligand (NPH_3^-). Additionally, the corresponding orbital energies for the imido (NH_2^-) and nitrido (N^{3-}) ligands are given for comparison. This plot results from EHT calculations.

Scheme 1



in the framework of Extended Hückel Theory (EHT).¹⁶ Accordingly, the highest occupied orbitals of the ligand are an *sp* lone-pair (a_1 symmetry) and a degenerate set of p orbitals (e symmetry). The latter are predominantly localized at the nitrogen atom but are slightly pushed up in energy due to a weak antibonding interaction with the PH_3 fragment.

For the OR^- , SR^- , or NR^{2-} ligands, which are isolobal to NPH_3^- , a similar sequence of orbitals can be observed. An analysis of the charge density utilizing the NBO partitioning scheme^{17,18} shows Lewis structure **A** to be most important in the free phosphorane-iminate ion. As a ligand coordinated to a transition metal ion, NPH_3^- becomes polarized. The negative charge at N increases while the N–P bond order decreases. Thus, the coordinated ligand should then be described by Lewis structure **B**. An accumulation of negative charge is stabilized by the neighboring transition metal centers, so the charge concentration on the nitrogen atom increases in the order $\mu_1 < \mu_2 < \mu_3$ coordination. This is demonstrated in Table 1 for the monomeric, dimeric, and tetrameric zinc complexes. According to the Wiberg bond indices the M–N bond is best described as an ionic interaction. For comparison the population analyses for the phosphorane-imine HNPH_3 and the *N*-silylphosphorane-imine H_3SiNPH_3 are given. These molecules show covalent, albeit strongly polar N–R ($\text{R} = \text{H}, \text{SiH}_3$) bonds. The pronounced ionic character of the transition metal nitrogen bond can also be visualized by a plot of the Laplacian of the charge density ($\nabla^2\rho(\vec{r})$),¹⁹ which clearly shows no charge concentration in the M–N binding region (see Figure 3).

(16) Landrum, G. A. YAeHMOP–Hückel Molecular Orbital Package, Version 2.0, URL: <http://overlap.chem.cornell.edu:8080/yaehmop.html>, Cornell University, 1997.

(17) Reed, A. E.; Curtiss, L. A.; Weinhold, F. *Chem. Rev.* **1988**, *88*, 899–926.

(18) Reed, A. E.; Weinstock, R. B.; Weinhold, F. *J. Chem. Phys.* **1985**, *83*, 735–746.

(19) Bader, R. F. W. *Atoms in Molecules*; Clarendon Press: Oxford, 1994.

Table 1. Population Analysis for Some Phosphorane–Iminato Compounds at Density Functional Level: NPA Charges (q) and Wiberg Bond Indices (b)

molecule	$q(\text{M})$	$q(\text{N})$	$q(\text{P})$	$b(\text{N–P})$	$b(\text{M–N})^a$
NPH_3^-		–1.399	+1.055	1.180	
HNPH_3	+0.368	–1.276	+1.132	1.349	0.843
H_3SiNPH_3	+1.201	–1.546	+1.217	1.253	0.733
$\text{ZnBr}(\text{NPH}_3)$	+1.353	–1.689	+1.191	1.308	0.419
$(\text{ZnBr}(\text{NPH}_3))_2$	+1.463	–1.853	+1.229	1.183	0.180
$(\text{ZnBr}(\text{NPH}_3))_4$	+1.469	–1.880	+1.217	1.124	0.125
$\text{CdBr}(\text{NPH}_3)$	+1.312	–1.612	+1.172	1.335	0.462
$(\text{CdBr}(\text{NPH}_3))_2$	+1.448	–1.795	+1.214	1.227	0.188
$(\text{CdBr}(\text{NPH}_3))_4$	+1.469	–1.828	+1.194	1.177	0.127

^aBond indices calculated for a single M–N bond.

2.2. Molecular Orbitals of the Heterocubane. One way to analyze the electronic structure of the heterocubanes in a qualitative manner is a decomposition of the molecular orbitals into fragment orbitals utilizing EHT.²⁰ This is depicted in Figure 4. Accordingly, heterocubane formation occurs due to stabilization of the highest occupied MOs of a hypothetical $(\text{NPH}_3^-)_4$ tetrahedron upon mingling with the unoccupied 4s, 4p, and 3d (5s, 5p in case of $\text{M} = \text{Cd}$) orbitals of the transition metal atoms. A direct intermetallic bond can be ruled out for the M–M distances found in the equilibrium structure of the cubanes (typically 2.8–3.0 Å)⁶ because of the very small energy splitting of the fragment orbitals in the $(\text{MBr})_4^{4+}$ tetrahedron.

The highest occupied MOs in the heterocubane are linear combinations of transition metal d orbitals whereas the lowest unoccupied MOs have transition metal s- and p-orbital character. Overall the heterocubanes should have a large HOMO–LUMO gap and a closed shell ground state can be assumed if the M^{2+} ions have completely filled d shells ($\text{M} = \text{Zn}, \text{Cd}$). Because of the small energy differences within the d band, high-spin complexes have to be expected for all other cases, but there is no simple way to deduce the multiplicity of the ground state on the basis of EHT calculations.

More insight into the electronic structure can be gained from a decomposition of the heterocubane as depicted in Figure 5. Instead of analyzing the MOs of the entire cubane it seems to be favorable to concentrate on the energy splitting of the d orbitals of just *one* transition metal ion in its *local* ligand field. By this approximation the interaction between the transition metal centers (through space or through the M–N bonds) is neglected. This can be justified by the observation that the energy splitting caused by the local ligand field is much larger than the effect of $\text{M}\cdots\text{M}$ interactions. As a result of the simplification each transition metal can be described in a local ligand field of C_{3v} symmetry. The apical position of this trigonal pyramid is occupied by the halide ion, the basal positions by the nitrogen atoms. The splitting of the d orbitals in this distorted tetrahedral ligand field is depicted in Figure 5. EHT calculations show that the overall splitting is in an order of magnitude of 1 eV: the ligand field is rather weak as one would expect for tetrahedral coordination. Thus, in the ground state the d electrons of each transition metal center are coupled high spin,

$$S_i = \sum_{i=1}^{n_\alpha} \frac{1}{2} \quad (1)$$

where n_α is the number of unpaired electrons of one transition metal center (i.e. 1 for Cu^{2+} , 2 for Ni^{2+} , 3 for Co^{2+} , 4 for Fe^{2+} , and 5 for Mn^{2+}) and S_i is the total spin moment of that atom.

(20) Albright, T. A.; Burdett, J. K.; Whangbo, M. H. *Orbital Interactions in Chemistry*; Wiley-Interscience: New York, 1985.

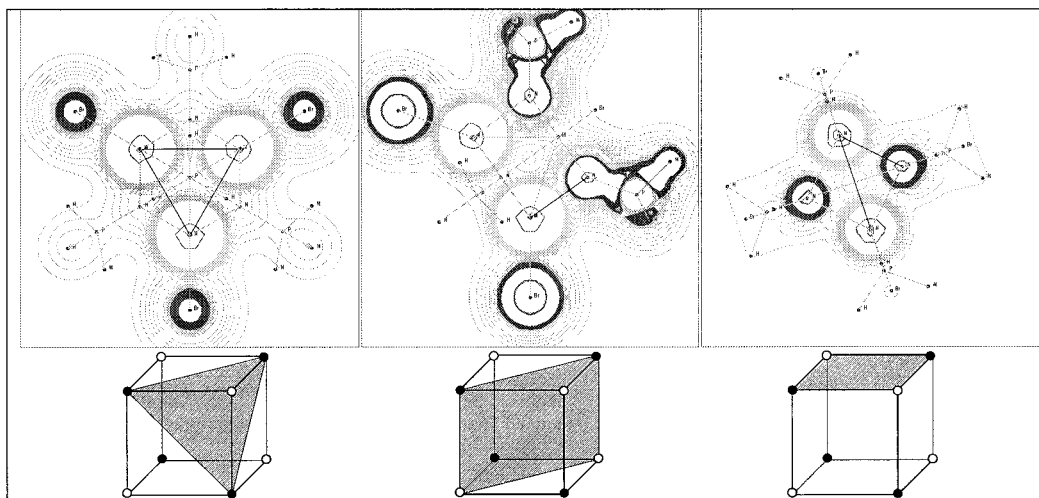


Figure 3. Contour plot of the Laplacian of the charge density ($\nabla^2\rho(\mathbf{r})$). Left: Plot in the plane of three transition metal atoms. Middle: The plotting plane contains the diagonals of two opposite faces. Right: Plot in the plane of one face of the cube. Black contours: $\nabla^2\rho(\mathbf{r}) < 0$, regions of local charge concentration. Gray contours: $\nabla^2\rho(\mathbf{r}) > 0$, regions of local charge depletion.

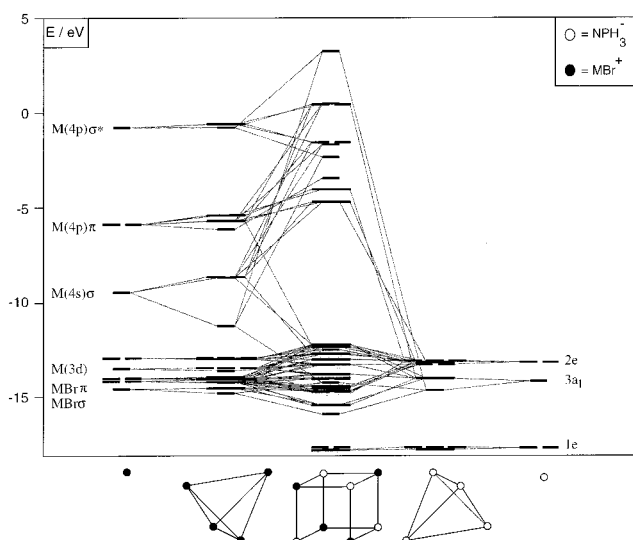


Figure 4. MO diagram for the interaction of a $(\text{NPH}_3)_4^{4-}$ tetrahedron with a $(\text{MBr})_4^{4+}$ tetrahedron. The orbitals that are occupied if the transition metal ions have a completely filled d shell are marked in gray. This scheme is the result of a EHT calculation.

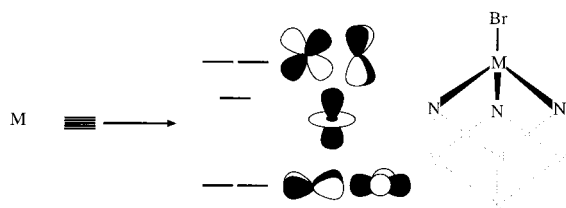


Figure 5. Energy splitting of the transition metal d orbitals in the local trigonal-pyramidal ligand field of one corner of the cube (with C_{3v} symmetry). EHT calculations show a total energy difference of ≤ 1 eV. If these d orbitals are occupied by 6 ($M = \text{Fe}$) or 9 ($M = \text{Cu}$) electrons, Jahn–Teller distortion has to be expected.

But what is the total spin moment of the entire heterocubane in its electronic ground state?

2.3. Spin Coupling in the Heterocubane. In a second step a Heisenberg Hamiltonian has been introduced to account for the weak interaction of the transition metal centers,^{21–24}

according to eq 2,

$$\hat{H} = - \sum_{i=1}^3 \sum_{j>i}^4 J_{ij} \mathbf{S}_i \mathbf{S}_j \quad (2)$$

where \mathbf{S}_i , \mathbf{S}_j are the total spin moments of two neighboring centers and the J_{ij} are the corresponding coupling constants between these centers.

For the highly symmetrical heterocubanes all J_{ij} can be assumed to have the same value “ J ”. Thus eq2 reduces to

$$\hat{H} = -J \sum_{i=1}^3 \sum_{j>i}^4 \mathbf{S}_i \mathbf{S}_j \quad (3)$$

which implies that some eigenvalues of this Hamiltonian are degenerate. With the relation

$$\sum_{i=1}^3 \sum_{j>i}^4 \mathbf{S}_i \mathbf{S}_j = \frac{1}{2} (\mathbf{S}^2 - \sum_{i=1}^4 \mathbf{S}_i^2) \quad (4)$$

the expectation values of the Heisenberg Hamiltonian for the heterocubanes are

$$E[\mathbf{S}] = -\frac{J}{2} (\langle \mathbf{S}^2 \rangle - \sum_{i=1}^4 \langle \mathbf{S}_i^2 \rangle) = -\frac{J}{2} (\mathbf{S}(\mathbf{S} + 1) - 4\mathbf{S}_i(\mathbf{S}_i + 1)) \quad (5)$$

In the second step of eq 5 we made use of the fact that the eigenvalues $\langle \mathbf{S}_i^2 \rangle$ of all four spin moments are identical. For this case, the allowed values for the total spin of the heterocubane are

$$\mathbf{S} = 4\mathbf{S}_i, 4\mathbf{S}_i - 1, \dots, 0 \quad (6)$$

and energy differences between two successive states can be written in the form

$$E[\mathbf{S} + 1] = E[\mathbf{S}] - J(\mathbf{S} + 1) \quad (7)$$

(21) Sinn, E. *Coord. Chem. Rev.* **1970**, *5*, 313–347.

(22) Griffith, J. S. *Struct. Bonding* **1972**, *10*, 87–126.

(23) Griffith, J. S. *Mol. Phys.* **1972**, *24*, 833–842.

(24) Hay, P. J.; Thibault, J. C.; Hoffmann, R. *J. Am. Chem. Soc.* **1975**, *97*, 4884–4899.

If the energies of the spin states are known, it is possible to determine the parameter J . This coupling constant will have a negative sign for an antiferromagnetic interaction leading to a singlet ground state.

3. Methodology

All molecules are fully optimized at ROHF and B3LYP²⁸ levels utilizing the effective core potential basis sets of Stevens, Basch, and Krauss,^{29,30} augmented by one set of polarization functions (of d type) for the heavy (non hydrogen) main group elements. The use of polarization functions is imperative to get a correct description of the strongly polar N–P bond. All stationary points were characterized as local minima by inspection of the eigenvalues of the corresponding Hessian matrices (calculated at ROHF and DFT levels).

The optimizations have been performed on the electronic state of the highest multiplicity possible in each case. This can be justified (a) by the small size of the antiferromagnetic interactions and (b) the fact that, even in their singlet ground state, the electrons are coupled high spin in the d shells of the transition metal atoms. Thus, the structural differences between the electronic states are expected to be of minor importance.

Starting from the ROHF wave function (at the ROHF equilibrium structure) CASSCF calculations have been performed to determine the electronic ground state of each multiplicity, according to eq 6. The energy differences between these states were mapped onto the states of the Heisenberg Hamiltonian to determine the size of the coupling constant J . The complete active space is spanned by the singly occupied orbitals/electrons of the ROHF determinant (e.g. for the cubane with $M = \text{Co}$ an active space of 12 electrons in 12 orbitals was used). This ensures a qualitatively correct wave function that is an eigenfunction of S^2 , but it neglects dynamical correlation. To account for effects of dynamical correlation, for all dimers and one heterocubane (with $M = \text{Ni}$) additional multireference perturbation theory calculations have been performed on all spin states. For this purpose the MCQDPT code of Nakano³¹ as implemented in the GAMESS set of programs³² was utilized. The DFT calculations were performed using the Gaussian 98 package.³³

4. Results of the Calculations

4.1. Molecular Structures. To get an estimate of the strength of the transition metal nitrogen bonds in the heterocubanes, we

(25) Wang, S. G.; Schwarz, W. H. E. *J. Chem. Phys.* **1998**, *109*, 7252–7262.

(26) McGregor, K. T.; Watkins, N. T.; Lewis, D. L.; Drake, R. F.; Hodgson, D. J.; Hatfield, W. E. *Inorg. Nucl. Chem. Lett.* **1973**, *9*, 423–428.

(27) de Loth, P.; Cassoux, P.; Daudy, J. P.; Malrieu, J. P. *J. Am. Chem. Soc.* **1981**, *103*, 4007–4016.

(28) Becke, A. D. *J. Chem. Phys.* **1993**, *98*, 5648–5653.

(29) Stevens, W. J.; Basch, H.; Krauss, M. *J. Chem. Phys.* **1984**, *81*, 6026–6033.

(30) Stevens, W. J.; Krauss, M.; Basch, H.; Jasien, P. G. *Can. J. Chem.* **1992**, *70*, 612–630.

(31) Nakano, H. *J. Chem. Phys.* **1993**, *99*, 7983–7992.

(32) Schmid, M. W.; Baldrige, K. K.; Boatz, J. A.; Elbert, S. T.; Gordon, M. S.; Jensen, J. H.; Koseki, S.; Matsunaga, N.; Nguyen, K. A.; Su, S.; Windus, T. L.; Dupuis, M.; Montgomery, J. A. *J. Comput. Chem.* **1993**, *14*, 1347–1363.

(33) Frisch, M. J.; Trucks, G. W.; Schlegel, H. B.; Scuseria, G. E.; Robb, M. A.; Cheeseman, J. R.; Zakrzewski, V. G.; Montgomery, J. A., Jr.; Stratmann, R. E.; Burant, J. C.; Dapprich, S.; Millam, J. M.; Daniels, A. D.; Kudin, K. N.; Strain, M. C.; Farkas, O.; Tomasi, J.; Barone, V.; Cossi, M.; Cammi, R.; Mennucci, B.; Pomelli, C.; Adamo, C.; Clifford, S.; Ochterski, J.; Petersson, G. A.; Ayala, P. Y.; Cui, Q.; Morokuma, K.; Malick, D. K.; Rabuck, A. D.; Raghavachari, K.; Foresman, J. B.; Cioslowski, J.; Ortiz, J. V.; Stefanov, B. B.; Liu, G.; Liashenko, A.; Piskorz, P.; Komaromi, I.; Gomperts, R.; Martin, R. L.; Fox, D. J.; Keith, T.; Al-Laham, M. A.; Peng, C. Y.; Nanayakkara, A.; Gonzalez, C.; Challacombe, M.; Gill, P. M. W.; Johnson, B.; Chen, W.; Wong, M. W.; Andres, J. L.; Gonzalez, C.; Head-Gordon, M.; Replogle, E. S.; Pople, J. A. *Gaussian 98*, Revision A.3; Gaussian, Inc.: Pittsburgh, PA, 1998.

(34) Schaftenaar, G. *Molden 3.4*, URL: <http://www.caos.kun.nl/schaft/molden/molden.html>, 1999.

Table 2. Selected Bond Lengths (in Å) and Angles (in deg) for MBr(NPH₃) Molecules

M, mult	method	M–N	M–Br	N–P	N–M–Br	M–N–P
Zn, 1	HF	1.782	2.269	1.520	179.7	174.8
	B3LYP	1.791	2.250	1.565	175.2	135.1
Cd, 1	HF	1.989	2.465	1.522	178.5	161.5
	B3LYP	2.007	2.450	1.569	174.6	132.3
Cu, 2	ROHF	1.784	2.297	1.524	180.0	176.1
	B3LYP	1.779	2.237	1.595	178.6	135.6
Ni, 3	ROHF	1.798	2.322	1.527	180.0	180.0
	B3LYP	1.738	2.243	1.562	179.2	175.5
Co, 4	ROHF	1.838	2.363	1.521	180.0	180.0
	B3LYP	1.758	2.262	1.561	179.9	179.8
Fe, 5	ROHF	1.856	2.397	1.525	180.0	180.0
	B3LYP	1.797	2.327	1.553	179.8	180.0
Mn, 6	ROHF	1.897	2.439	1.525	180.0	180.0
	B3LYP	1.837	2.369	1.552	180.0	179.9

assumed the hypothetical molecules MBr(NPH₃) and [MBr(NPH₃)₂] to be building blocks of the cubic structures. In more detail, we will analyze the metal–nitrogen bonding in three steps, in the formation of monomers, dimers, and finally the cubane structures.

4.1.1. Monomers. On one hand such monomers are expected to be highly reactive. They are experimentally unknown. On the other hand, the dihalides of the transition metals of the 3d series (MCl₂ or MF₂) exist at high temperatures in the gas phase. These molecules have been subject to a recent study utilizing DFT methods.²⁵ All molecules containing elements relevant for this study (Mn, Fe, Co, Ni, Cu, Zn) are reported to be high-spin complexes with a linear structure. According to our calculations, the same holds true for the phosphorane–iminato complexes. The Br–M–N bond angle is found to be linear in all cases, but only small vibrational frequencies (130–150 cm⁻¹) were determined for the Br–M–N deformation. This is in accordance with the findings made for the dihalides (MCl₂, 70–110 cm⁻¹; MF₂, 120–180 cm⁻¹).²⁵ The M–N–P angle is very floppy ($\nu_{\text{def}} = 8\text{--}55\text{ cm}^{-1}$), too. An explanation for this is the weak π -acceptor character of a 3d transition metal in the oxidation state +2. For the d¹⁰ and d⁹ complexes ($M = \text{Zn/Cd}$ and $M = \text{Cu}$, respectively) a bond angle of 135° is found, all other complexes have almost linear M–N–P angles. The optimized structural parameters are given in Table 2.

4.1.2. Dimeric Structures. The first step of heterocubane formation starting from the monomers MBr(NPH₃) is the dimers [MBr(NPH₃)₂]. Our calculations show that these molecules adopt the structure of a planar, almost quadratic M₂N₂ ring. Because of the orientation of the PH₃ groups the overall symmetry is lowered to point group C₂. Although such dimers could not be isolated (they should be strong acceptors for both Lewis acids and Lewis bases, because the transition metal atoms and the nitrogen atoms are unsaturated), there is some evidence for dimeric fragments in the mass spectra of the heterocubanes.⁶ With respect to our computational study these dimers are important because the spin coupling phenomena are much easier to investigate in detail for these smaller molecules than for the heterocubanes themselves. For completeness some parameters describing the equilibrium structures are given in Figure 6.

4.1.3. Heterocubane Structures. For the heterocubanes some optimized structural parameters are given in Figure 7. For comparison experimental data from crystal structure determinations are also given. All structures are optimized for the electronic state of the highest multiplicity possible for each transition metal ion. All molecules have D_{2d} symmetry with a nearly ideal cubic structure. Only for the d⁹ ($M = \text{Cu}^{2+}$) and d⁶ configuration ($M = \text{Fe}^{2+}$) can a distortion of the M₄N₄ core be

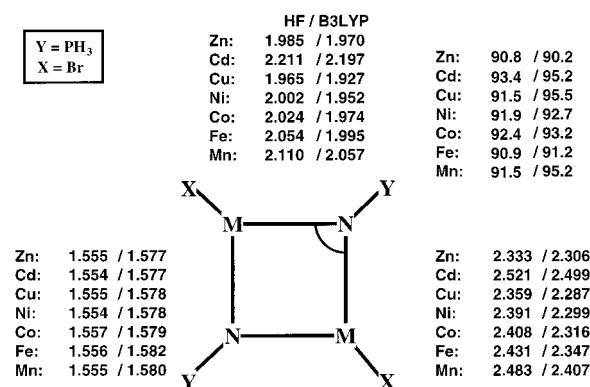


Figure 6. Selected bond lengths (in Å) and angles (in deg) for dimers ($[\text{BrMnPH}_3]_2$).

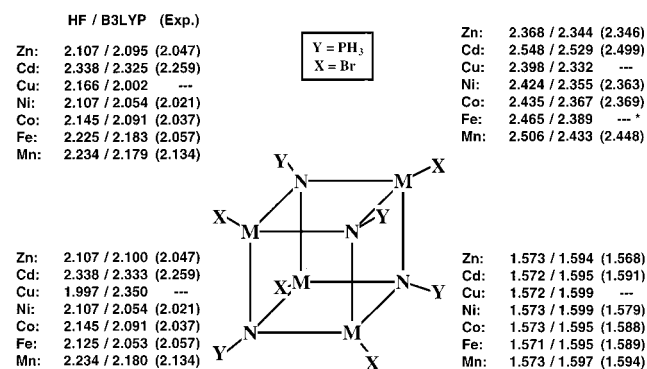


Figure 7. Selected bond lengths (in Å) and angles (in deg) for heterocubanes ($[\text{BrMnPH}_3]_4$). High spin complexes have been assumed for all calculations. Experimental parameters⁶ are given in parentheses. Asterisk: For $M = \text{Fe}$ the experimental values refer to a complex with $X = \text{Cl}$ instead of Br .

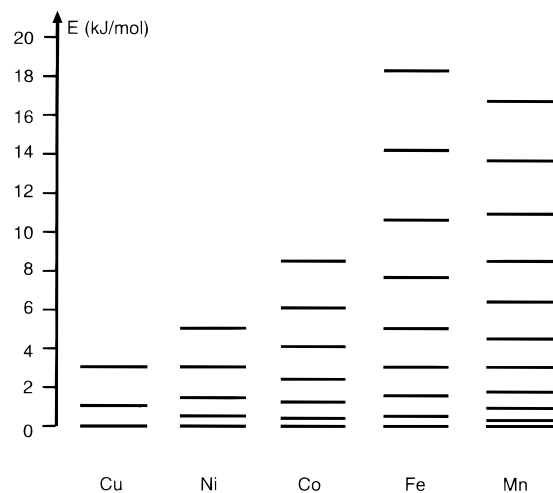


Figure 8. Expectation values of the Heisenberg Hamiltonian for the heterocubanes. The calculated/estimated values of J (as given in the text) were used to determine the spin ladders.

observed: one short and two long $M-N$ bonds were found for each transition metal center. According to the MO scheme depicted in Figure 5, this observation can be explained as a Jahn–Teller distortion: If the d shell of a transition metal atom in a C_{3v} symmetrical ligand field is occupied by six or nine d electrons, a degenerate ground state results. The molecular structure is unstable toward a distortion that destroys the 3-fold symmetry axis and removes the degeneracy. This is evidenced by the computational results.

Table 3. Stabilization Energies per Monomer (in $\text{kJ}\cdot\text{mol}^{-1}$) for the Association of Hypothetical $\text{MBr}(\text{NPH}_3)$ Units

M		$\Delta E(\text{dimer})$	$\Delta E(\text{tetramer})$
Zn	HF	−110.4	−168.2
	B3LYP	−95.0	−142.9
Cd	HF	−103.9	−153.6
	B3LYP	−83.0	−127.5
Cu	HF	−146.3	−177.1
	B3LYP	−77.7	−96.2
Ni	HF	−146.3	−226.4
	B3LYP	−105.3	−159.7
Co	HF	−127.3	−202.6
	B3LYP	−95.1	−152.9
Fe	HF	−116.7	−166.2
	B3LYP	−106.7	−139.7
Mn	HF	−119.6	−185.6
	B3LYP	−103.1	−158.7

Our calculated structural parameters are in quite good agreement with the experimental ones. The $M-N$ bond lengths are systematically overestimated by about 3% at the DFT level (<5% at HF level) for the closed shell and the open shell cases. So we can be confident that our assumptions for the spin state (high spin coupling in the d shell) were correct. Additionally, the calculations indicate that the cubane structure is intrinsic to the molecules and not an effect of crystal structure packing. A comparison of the $M-N$ and the $M-Br$ distances in dependence of the choice of the transition metal shows the usual trends in the ionic radii of M^{2+} ions of the 3d series. The same trend can be observed for the experimental structures. The $N-P$ distances on the other hand turn out to be almost independent of the nature of the transition metal.

5. Energetic Considerations

The stabilization energies of the dimers ($n = 2$) and the heterocubanes ($n = 4$) with respect to the hypothetical reaction $n\text{MBr}(\text{NPH}_3) \rightarrow [\text{MBr}(\text{NPH}_3)]_n + n\Delta E$ are given in Table 3. All cubanes were calculated to have stabilization energies per monomeric unit in a range of 130 to 160 $\text{kJ}\cdot\text{mol}^{-1}$ (calculated at the DFT level).

The size of these energies is supported by the experimental finding that molecular ions can be detected with high relative intensity in the mass spectra.⁶ The largest amount of stabilization energy is gained upon dimerization (about 2/3). The additional third $M-N$ bond formed upon tetramerization has only the strength of 40–50 $\text{kJ}\cdot\text{mol}^{-1}$ per monomer. Thus, one should expect some tendency for decomposition into two dimers. Probably, the cleavage of the cubane structure can be enforced by addition of sufficiently strong donors for binding to the transition metal centers. Interestingly, the stability of the copper compound toward dissociation into two dimers is very small. This is another effect of the Jahn–Teller distortion. The instability is a possible reason why a heterocubane with $M = \text{Cu}$ could not be synthesized so far. A less pronounced reduction in the stabilization energy is also found for the iron complex.

6. Calculated Coupling Constants

6.1. Dimers. For the dimers a good mapping between the states of the ab initio Hamiltonian and the Heisenberg Hamiltonian (compare ΔE with $\Delta E_j(\mathbf{S})$ in Table 4) is found. Maximum deviations are about 5%, so the simple model Hamiltonian seems to be sufficient to describe the electronic structure.

The calculations reveal an antiferromagnetic interaction of the transition metal centers (i.e. the coupling constants J have a negative sign). This corresponds to a singlet ground state for

Table 4. Relative Energies for the Spin States of the Dimers (in $\text{kJ}\cdot\text{mol}^{-1}$)^a

	S	2S + 1	ΔE	$E(J)$	J	$\Delta E_J(\text{S})$
Cu	0	1	0.0	0J		0.0
	1	3	1.41 (3.22)	1J	-1.41 (-3.22)	1.41 (3.22)
Ni	0	1	0.0	0J		0.0
	1	3	0.34 (0.85)	1J	-0.32 (-0.79)	0.32 (0.79)
	2	5	0.93 (2.32)	3J		0.98 (2.37)
Co	0	1	0.0	0J		0.0
	1	3	0.21 (0.65)	1J		0.20 (0.58)
Fe	2	5	0.61 (1.84)	3J	-0.20 (-0.61)	0.60 (1.74)
	3	7	1.13 (3.34)	6J		1.20 (3.48)
	0	1	0.0	0J		0.0
	1	3	0.32(0.98)	1J		0.29 (0.90)
	2	5	0.93 (2.85)	3J	-0.29 (-0.90)	0.87 (2.70)
Mn	3	7	1.79 (5.47)	6J		1.74 (5.40)
	4	9	2.84 (8.61)	10J		2.90 (9.00)
	0	1	0.0	0J		0.0
	1	3	0.26 (0.60)	1J		0.19 (0.54)
Mn	2	5	0.63 (1.72)	3J		0.57 (1.62)
	3	7	1.17 (3.34)	6J	-0.19 (-0.54)	1.14 (3.24)
	4	9	1.85 (5.38)	10J		1.90 (5.40)
	5	11	2.65 (7.74)	15J		2.85 (8.10)

^a The results of CASSCF/SBK(d)//ROHF/SBK(d) and MCQDPT/SBK(d)//ROHF/SBK(d) (in parentheses) calculations are given. S: total spin moment. (2S + 1): multiplicity. ΔE : energy relative to the (singlet) ground state. $E(J)$: corresponding expectation value of the Heisenberg Hamiltonian (in multiples of J). J : coupling constant determined by fitting the ab initio result. $\Delta E_J(\text{S})$: expectation values of the Heisenberg Hamiltonian using the calculated J .

all molecules, but the interactions are rather small, as is witnessed by the small values of J . Therefore, states of higher multiplicity will become thermally populated at room temperature. For example, in the dimer with $M = \text{Cu}$ the calculated value of J is $3.22 \text{ kJ}\cdot\text{mol}^{-1}$ ($=270 \text{ cm}^{-1}$). Coupling constants of comparable size have been found for the classical μ_2 -OH bridged dimeric copper complexes.^{24,26,27}

Furthermore, the results show that the neglect of dynamical correlation introduces a systematic error. The size of J resulting from a CASSCF calculation is only 33% of the MCQDPT result. This deviation is nearly independent of the nature of the transition metal. Thus, an extrapolation from the CASSCF values seems to be acceptable for these systems to estimate the magnitude of J in cases where the MCQDPT method is too demanding.

6.2. Heterocubanes. Our calculated coupling constants for the heterocubanes are only half as large as those for the corresponding dimers. Since $M\cdots M$ coupling occurs via the $M-N$ bonds, this can be explained by the longer $M-N$ bonds in the cubane, which are found to be about 0.1 \AA (for $M = \text{Cu}$ 0.2 \AA) longer than in the dimers. Because of the immense amount of computer resources needed for MCQDPT calculations on the heterocubanes, only calculations for the spin states of the nickel compound have been performed. It turns out that CASSCF calculations give coupling constants of only 33% of the MCQDPT value. This was also found for the dimers. Thus, an extrapolation from the CASSCF results seems to be reasonable for $M = \text{Cu}$, Co . The estimates are $J(\text{Cu}) \approx 1.0 \text{ kJ}\cdot\text{mol}^{-1}$ and $J(\text{Co}) \approx 0.4 \text{ kJ}\cdot\text{mol}^{-1}$. For the elements iron and manganese even CASSCF calculations are out of reach because the corresponding active space becomes too large. Only estimates from coupling constants calculated for the dimers are possible. For the nickel and cobalt complexes coupling constants in the

Table 5. Relative Energies for the Spin States of the Heterocubanes (in $\text{kJ}\cdot\text{mol}^{-1}$) (CASSCF/SBK(d)//ROHF/SBK(d) and MCQDPT/SBK(d)//ROHF/SBK(d) (in parentheses))^a

	S	2S + 1	ΔE	$E(J)$	J	$\Delta E_J(\text{S})$
Cu	0	1	0.0	0J		0.0
	1	3	0.35	1J	-0.33	0.33
	2	5	0.95	3J		0.99
Ni	0	1	0.0	0J		0.0
	1	3	0.16 (0.57)	1J		0.15 (0.50)
	2	5	0.50 (1.73)	3J	-0.15 (-0.50)	0.45 (1.50)
	3	7	0.92 (3.06)	6J		0.90 (3.00)
Co	4	9	1.48 (4.73)	10J		1.50 (5.00)
	0	1	0.0	0J		0.0
	1	3	0.11	1J		0.13
	2	5	0.39	3J		0.39
	3	7	0.80	6J	-0.13	0.78
	4	9	1.31	10J		1.30
	5	11	1.93	15J		1.95
6	13	2.65	21J		2.73	

^a The symbols have the same meaning as in Table 4.

cubanes are about 60% smaller than those in the dimer. Transferring this to the complexes of iron and manganese leads to estimated coupling constants of $J(\text{Fe}) \approx 0.5 \text{ kJ}\cdot\text{mol}^{-1}$ and $J(\text{Mn}) \approx 0.3 \text{ kJ}\cdot\text{mol}^{-1}$. Though it is not possible to determine accurate values for J in these molecules, the results calculated for the dimers can be considered at least as upper bounds. Coupling in the heterocubanes should be expected to be smaller. Our calculations demonstrate that there is only a weak antiferromagnetic interaction, but even this small coupling constant results in a splitting of energy levels that prevents the population of states of high multiplicity at room temperature. This finding is sufficient to explain the reduced magnetic moment observed in the experiment.

7. Summary

The results of our calculations can be summarized as follows:

1. The molecular structure of the heterocubanes can be reproduced by quantum chemical calculations performed on their high-spin states.

2. According to our analysis of the charge density, the transition metal nitrogen bonds have to be characterized as ionic interactions.

3. The short $N-P$ bonds are best described as strongly polar single bonds. There is no significant multiple bond character found, but the charge separations between nitrogen and phosphorus atoms are rather large.

4. An analysis of the spin states reveals the heterocubanes to be clusters of high-spin complexes. All unpaired electrons are localized in the d shells of the transition metal atoms. The transition metal centers are coupled by weak antiferromagnetic interactions. Thus, the spin states can be represented in the framework of the isotropic Heisenberg model. Our calculated coupling constants J are rather small. This weak coupling seems to be sufficient to explain the reduced magnetic moments observed in experimental studies. Since temperature-dependent susceptibility measurements have not been reported for this class of compounds, however, a comparison with experimental J values is not possible.

Acknowledgment. This work has been supported by the Deutsche Forschungsgemeinschaft and the Fonds der Chemischen Industrie.